

Chain Conformation and Aggregation Structure Formation of a High Charge Mobility DPP-Based Donor–Acceptor Conjugated Polymer

Chang Liu, Wenxian Hu, Hanqiu Jiang, Guoming Liu,* Charles C. Han, Henning Sirringhaus, François Boué,* and Dujin Wang

Cite This: *Macromolecules* 2020, 53, 8255–8266

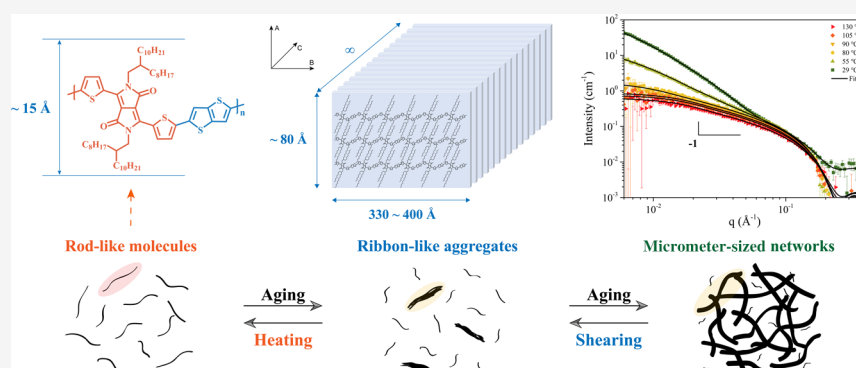
Read Online

ACCESS |

Metrics & More

Article Recommendations

Supporting Information



ABSTRACT: The determination of intrinsic chain stiffness of conjugated polymers is challenging, in particular, for scattering techniques because of their strong light absorption and structural instability due to the complicated intra-/intermolecular interactions. In this work, the chain conformation and aggregation formation of a high charge mobility donor–acceptor polymer (DPPDTP) are systematically investigated by using small-angle neutron scattering (SANS) and static/dynamic light scattering (SLS/DLS). On the one hand, chloroform was chosen as a good solvent, in which SANS reveals a rod-like geometry with a radius of ~ 15 Å. Once the absorption effect is properly accounted for, SLS shows a power law of 1 between the radius of gyration (R_g) and molecular weight (M_w) and a negative second virial coefficient (A_2). On the other hand, 1,2-dichlorobenzene was chosen as a poor solvent, in which SANS, SLS/DLS, and atomic force microscopy (AFM) reveal a strong temperature-/concentration-dependent assembling behavior. The results provide a general picture of the multiscale assembly process of conjugated polymers.

1. INTRODUCTION

Conjugated polymers have been intensively investigated as the base material for optoelectronic devices^{1–3} owing to their excellent solution processability and mechanical robustness. The semiconducting properties come from the delocalization of π -electrons, giving rise to the fastest transport of charge carriers along the backbone. The final solid-state morphology and molecular organization, governed by the chemical structure as well as processing parameters during solvent evaporation, are of great significance on the determination of the physical properties of conjugated polymers.^{4,5} However, the impact of backbone rigidity started only recently to attract attention for structural assembly,⁶ charge transport,^{7–11} and optical absorption and photoluminescence,^{12,13} although the molecular design has already shown a preference of monomers with fused rings and bulky side chains.^{14,15} Theories have correlated charge mobility with persistence length (L_p).^{7–9} More rigid backbones, among which coplanar ones, with maximized overlapping of wave functions, should facilitate a pathway for carrier transport. Many observations show a rather

similar evolution of L_p and the conjugation length. For example, experiments on poly(phenylene vinylene) (PPV) derivatives indicate that the increase in chain stiffness can significantly improve photoluminescence.¹⁶ However, a direct link between chain rigidity and optoelectronic properties has not been established yet.

As an essential characteristic of polymers, the chain conformation of some conjugated polymers was studied a long time ago.^{17,18} The privileged tool is small-angle neutron scattering (SANS) since the transition from rod-like at a small length scale and coil-like at a large length scale can occur within the accessible size range (L_p , a few nm to a few tens of nm) following the so-called worm-like chain behavior. A

Received: July 16, 2020

Revised: September 16, 2020

Published: October 1, 2020



pioneer work tackled the case of rather high L_p for polydiacetylene (poly-3 and -4 BCMU), with L_p close to 30 nm.¹⁹ Studied with the same SANS technique, poly(3-alkylthiophene) (P3AT)¹⁸ exhibits a statistical length of 5.5 nm, equivalently $L_p = 2.75$ nm, which is 2–3 times that of polystyrene ($L_p = 0.9$ – 1 nm);^{20,21} the most interesting is the rigidification when introducing dopants.¹⁸ The L_p values agree with a more recent wider SANS study for different poly(3-alkylthiophene) showing comparison with the behavior of the conjugation lengths under the influence of different alkyl lengths, synthesis routes, and the temperature.²² The L_p values for P3AT agree well also with former static/dynamic light scattering (SLS/DLS) studies where a worm-like conformation is also used for the analysis.^{23,24} The flexibility of the backbone arises from the distribution of syn and anti conformations as well as significant backbone torsion in polythiophenes. This results in a shorter persistence length than the estimated conjugation length, opposite to many other common conjugated polymers. In stiffer polymers, using SLS and DLS, worm-like chain behavior has also been reported, like for poly(*p*-phenylene-*cis*-benzobisoxazole) (*cis*-PBO, $L_{ps} = 19$ nm for high ionic strength and ~ 32 nm for low ionic strength)²⁵ and poly(phenyleneethynylenes) (PPE, $L_{ps} = 15$ nm).²⁶ Moreover, the predicted L_p of poly(3-hexylthiophene) (P3HT) by calculating the dihedral potentials is 2.8–4.0 nm, which agrees with experiments.^{9,10,27,28}

Another structural aspect is the intra-/interchain non-covalent interactions such as π – π interactions, which can lead to aggregation in solution.^{29,30} In this case, the solvent is considered as bad, but this is often temperature-dependent. Studying by SANS, both chain conformation in a good solvent and aggregation in a bad solvent are a burden since the earliest articles.¹⁹ However, other papers considered aggregation only, either because it is interesting for polymer systems, as they are often associated with an interesting gelification behavior,³¹ or because it is an important feature for conjugated polymer film casting, which is the most common practical application. This is the case, using SANS, for poly(2,3-diphenyl-5-hexyl-1,4-phenylenevinylene) (DP10-PPV)³² and DP6-PPV.³³ Other studies involved light scattering,^{34,35} small-angle X-ray scattering,³⁶ and UV–visible absorption spectra.^{37,38} It has been reported in the literature that the solution properties will shape the solid-state microstructure of polymer films and in turn largely influence the optoelectronic properties.^{39–43} However, most of the previous studies focused on the effect of processing conditions (such as different solvents) and thermal annealing directly on the final microstructure in solid state.

In this work, we consider the high-performance donor–acceptor (D-A)-type polymers. They contain monomers with alternating electron-rich and electron-deficient units. Their predicted L_p is 8 nm or greater (it even reaches 1 μm), indicating that it is likely to have an important influence on their optoelectronic properties.¹⁰ Strong π – π and donor–acceptor interactions make it easier to form aggregate structures in solution, even in the considered good solvent.^{30,44,45} This is accompanied by a high charge mobility and excellent characteristics for p-type field-effect transistors (FET).⁴⁶ We studied poly[3,6-bis(5-thiophen-2-yl)-2,5-bis(2-octyldodecyl) pyrrolo [3,4-*c*]pyrrole1,4(2H,5H)-dione-2,2'-diyl-*alt*-thieno[3,2-*b*]thiophen-2,5-diyl] (DPPDTT) (Figure 1a, with a predicted L_p of ~ 7.9 nm, more than twice that of P3HT) in solution by static/dynamic light scattering (SLS/

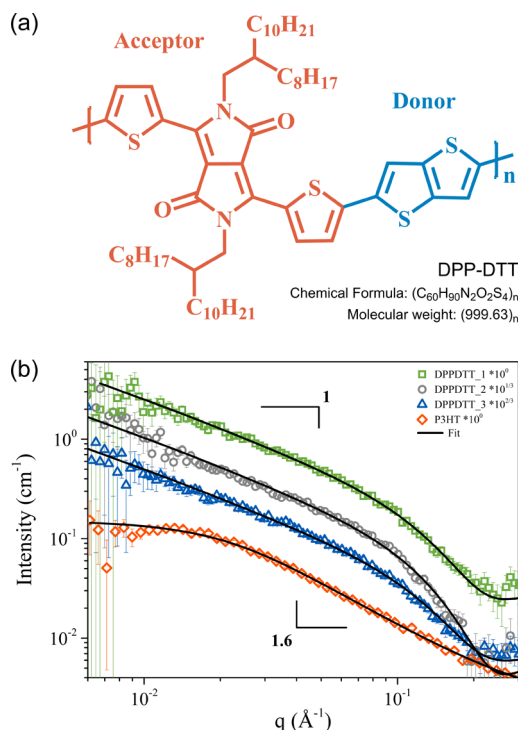


Figure 1. (a) Structural formula of DPPDTT. (b) SANS curves of three DPPDTT samples in CF-d (10 g/L) together with a P3HT sample in *o*-DCB- d^4 (5 g/L) measured at RT, in red hollow diamonds (the curves of DPPDTT_1 & 2 are multiplied by a constant: $10^{2/3}$ & $10^{1/3}$, respectively).

DLS), to uncover both chain conformation and the aggregation formation for the first time. This was complemented by temperature-varied SANS technique and atomic force microscopy observations and UV–vis spectroscopy.

2. EXPERIMENTAL SECTION

2.1. Materials and Sample Preparation. Three fractions of donor–acceptor copolymer DPPDTT were purchased from 1-Material, Inc., which were coded as DPPDTT_1, DPPDTT_2, and DPPDTT_3. P3HT ($M_w = 35$ kg/mol, PDI = 1.7, regioregular, electronic grade) was purchased from Sigma-Aldrich Co., Ltd. They were used as received without further purification. HPLC-grade chloroform (CF) and 1,2-dichlorobenzene (*o*-DCB) were purchased from Xilong Scientific Co., Ltd. Deuterated chloroform (CF- d , 99.8 atom % d) and 1,2-dichlorobenzene- d^4 (*o*-DCB- d^4 , 98 atom % d) were purchased from Innochem. Detailed information about the sample preparation can be found in the Supporting Information.

2.2. Small-Angle Neutron Scattering (SANS). SANS experiments were conducted at the China Spallation Neutron Source (CSNS) located at Dongguan, China. A sample-to-detector distance of 2.5 m was adopted, covering a q range of 0.005–0.45 \AA^{-1} . The scattering intensity was corrected for detector sensitivity. The scattering contribution from empty quartz cells and the solvent was subtracted. To fit the data, form factors of cylinder⁴⁷ and parallelepiped⁴⁸ were applied (details of the expressions can be found in the Supporting Information).

2.3. Static Light Scattering (SLS) Measurements. SLS/DLS measurements were conducted using a static/dynamic compact goniometer (SLS/DLS-5000, ALV, Langen, Germany) and a 100 mW solid laser operating at 532 nm (LMX-532, Oxixus, France) as the light source.

For SLS measurements, the scattering intensity was measured stepwise covering an angular range of 30–150°. The temperature of the sample was set at 25.0 (± 0.5 °C). Toluene was used as the standard to determine the absolute scattering of the sample. The

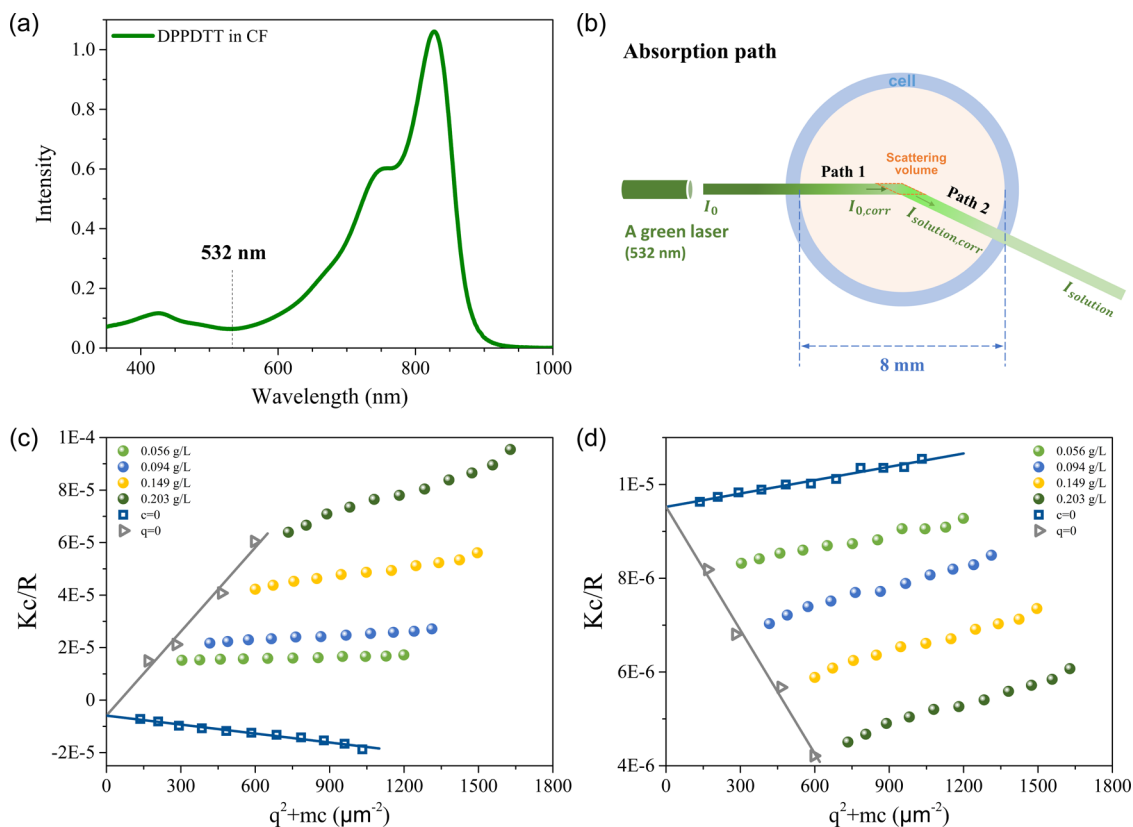


Figure 2. (a) UV–vis spectra of DPPDTT in CF at 25 °C. (b) Schematic diagram of the light absorption process. (c) Zimm plot of the raw SLS data of DPPDTT_1 in CF (at 25 °C) and (d) Zimm plot of the same data after correcting intensity from light absorption ($m = 3000$ in abscissa).

absolute weight-average molecular weight (M_w), the z -average mean radius of gyration (R_g), and the second virial coefficient (A_2) were determined by the extrapolation of Hc/R to $q = 0$ and $c = 0$ according to the relation⁴⁹

$$\frac{Hc}{R(q)} = \frac{1}{M_w} \left(1 + \frac{1}{3} q^2 R_g^2 + \dots \right) + 2A_2 c \quad (1)$$

where

$$q = \frac{4\pi n}{\lambda} \sin \frac{\theta}{2}, H = \frac{4\pi^2}{N_A \lambda^4} n^2 \left(\frac{dn}{dc} \right)^2 \quad (2)$$

dn/dc is the refractive index increment (1.0 mL/g for DPPDTT in CF as determined by a differential refractometer), n is the refractive index of the solvent (1.4476 for CF), c is the concentration of solutions, N_A is Avogadro's number, and λ is the vacuum wavelength of light. $R(q)$ is the excess Rayleigh ratio

$$R(q) = \frac{I_s(\theta) r^2}{I_0 V_s(\theta)} = \frac{I_{\text{solution}}/I_{0,\text{solution}} - I_{\text{solvent}}/I_{0,\text{solvent}}}{I_{\text{std}}/I_{0,\text{std}}} R_{\text{std}} \quad (3)$$

I_s is the excess scattering intensity (the difference between solution and pure solvent), r is the distance between the detector and the scattering volume, I_0 is the intensity of incident light, $V_s(\theta)$ is the scattering volume ($V_0/\sin(\theta)$), R_{std} is the Rayleigh ratios of toluene. In the form of a Zimm plot (Hc/R versus $q^2 + mc$), the parameters M_w , R_g , and A_2 can be obtained via extrapolation

$$\lim_{c \rightarrow 0} \frac{Hc}{R(q)} = \frac{1}{M_w} \left(1 + \frac{1}{3} q^2 R_g^2 \right) \quad (4)$$

$$\lim_{\theta \rightarrow 0} \frac{Hc}{R(q)} = \frac{1}{M_w} + 2A_2 c \quad (5)$$

2.4. Dynamic Light Scattering (DLS) Measurements. The concentration of DPPDTT solution used here was in the range of 0.05–0.20 g/L. Because of the low concentration of samples, the DLS experiments were conducted at a fixed low angle (20°) only, for the sake of time and accuracy. The correlation analysis was performed using the CONTIN method.

The rate of change in scattering intensity is quantified as an integral over the product of intensities at some time and with a delay time, and fluctuations in scattering intensity are recorded and converted into the intensity autocorrelation function $G^{(2)}(\tau)$

$$G^{(2)}(\tau) = \lim_{T \rightarrow \infty} \frac{1}{T} \int_0^T I(t)I(t + \tau) dt = \langle I(0)I(\tau) \rangle \quad (6)$$

The Siegert relation⁵⁰ connects the normalized intensity autocorrelation function $g^{(2)}(\tau) = G^{(2)}(\tau)/G^{(2)}(0)$ to the electric field time correlation function $g^{(1)}(\tau)$

$$g^{(2)}(\tau) = 1 + \beta |g^{(1)}(\tau)|^2 \quad (7)$$

Here, β is the spatial coherence factor, which is less than 1. For a monodisperse system undergoing the Brownian motion, $g^{(1)}(\tau)$ decays as an exponential with a decay rate Γ : $g^{(1)}(\tau) = \exp(-\Gamma\tau)$, where Γ is related to the diffusivity D by $\Gamma = Dq^2$. For a polydisperse system,⁵¹ $g^{(1)}(\tau)$ is related to the distribution $A(\Gamma)$ by

$$g^{(1)}(\tau) = \int_0^\infty A(\Gamma) \exp(-\Gamma\tau) d\Gamma \quad (8)$$

Also, in the case of Brownian motion, the average hydrodynamic radius (R_h) is obtained by the Stokes–Einstein equation

$$R_h = \frac{k_B T}{6\pi\eta D} \quad (9)$$

where k_B is the Boltzmann constant, T is the Kelvin temperature, and η is the viscosity.

2.5. dn/dc Measurements. The specific refractive index increment (dn/dc) of DPPDTT in CF was determined by a differential refractometer (AYE DN/DC-19 refractometer) at 25 °C.

2.6. Absorption Measurements. An ultraviolet–visible spectrophotometer (Lambda 950, PerkinElmer) was used to determine the absorption spectrum of DPPDTT.

2.7. Atomic Force Microscopy. AFM experiments were performed using a Multimode8 Bruker instrument by peak force tapping mode. The samples were prepared by spin-coating different solutions on a silicon wafer.

3. RESULTS AND DISCUSSION

3.1. SANS and SLS of DPPDTT in CF. CF and *o*-DCB are the two mostly used solvents for DPPDTT. It has been shown that DPPDTT has a high solubility in CF at room temperature (RT), whereas it can dissolve in *o*-DCB at high temperatures (~130 °C) only.^{11,46} Let us first discuss the SANS results in Figure 1b for the two cases where chains appear as well solubilized, (i) for three DPPDTT samples dissolved in deuterated CF and (ii) the P3HT sample dissolved in deuterated *o*-DCB. We fitted the DPPDTT data by a cylinder form factor⁴⁷ (P_{cyl}), which is given in the Supporting Information. On the contrary, we find that the P3HT scattering at a high q limit can be best fitted after considering the excluded volume effect ($I \approx q^{-1.6}$). This corresponds to a flexible chain with self-avoiding walk conformation (slightly different from the random walk Gaussian chain conformation reported formerly in the literature,²² $I \approx q^{-2}$ at a high q limit). Very differently, for DPPDTT in CF, the scattering intensity shows q^{-1} for $q < 10^{-1} \text{ \AA}^{-1}$ and down to the lowest q . This is a rod-like behavior, suggesting that the chain can be semiflexible, but with a very large persistence length exceeding the length range accessible with our SANS instrument. The minimum q value that the instrument can reach is about 0.005 \AA^{-1} , which is much larger than the required q for contour length of the chains. For $q > 10^{-1} \text{ \AA}^{-1}$, we observe a crossover to a sharp intensity drop. That corresponds to a length scale of 1 nm ($q = 0.1 \text{ \AA}^{-1}$ at the crossover), which coincides with the lateral size of the chain. Therefore, the curves were fitted with a form factor of cylinder. We assumed an “infinitely large” length (100 nm) because the scattering is not sensitive to the chain size in this q range. The cause of the extended conformation may be related to the hindrance of bond rotation by the bulky side chains. Moreover, no structure factor is observed, although they are above $c^*(L)$ (see the Supporting Information). It is important to note that under these conditions, in CF, no sign of aggregate was seen by SANS, which will be further discussed later.

To measure the global size of the chains, we need to reach the Guinier region of the scattering objects, which requires a smaller q . SLS can provide this access in dilute solutions since it covers a q range of $0.0009\text{--}0.003 \text{ \AA}^{-1}$. However, to ensure the stability of the solution, DLS measurements were performed first. As shown in Figure S3a, the sample shows a single decay in the autocorrelation function ($g^{(2)}(\tau) - 1$), and the feature remains unchanged for 144 h (at 25 °C) and at various temperatures. Here, we present the results of the SLS measurement at 25 °C.

Prompted by the strong coloration of the solution, we were concerned by the possibility that SLS measurements could be biased by absorption. We performed UV–vis measurements on DPPDTT/CF solutions. Figure 2a shows the spectrum, indicating strong light absorption in the visible range. To minimize this absorption, in SLS measurements, a green laser

(532 nm, coinciding with the minimum in the absorption spectrum of DPPDTT) was selected, and the experiments were performed at low concentrations (0.05, 0.10, 0.15, and 0.20 g/L, Figure S2a). Under these conditions, the transmittance (varies from 70 to 25% at an optical path of 4 mm) was determined by UV–vis. The Zimm plot of the raw data, shown in Figure 2c, leads to unphysical negative M_w and R_g due to the strong absorption. Therefore, correction of the intensity has to be carried out.

The correction of the data is carried out by considering the effect of absorption. Using the measurements just described, the concentration-absorbance relation was fitted by $A = Kbc$ (Figure S3b), where $A = \log(1/T) = \log(I_{\text{in}}/I_{\text{trans}})$, K is the absorption coefficient ($L/(g \text{ cm})$), and b is the optical path (0.4 cm). A relatively accurate absorbance of each concentration solution was obtained. Figure 2b illustrates the light path in a column cell with an 8 mm inner diameter; the absorption occurs both in the incident (path 1) and scattering (path 2) direction with a 4 mm path each. In the direction of incident light, incident light has to travel 4 mm in the solution before reaching the scattering volume. So, the incident intensity has to be corrected

$$I_{0,\text{corr}} = I_{0,\text{solution}} \times 10^{-A} \quad (10)$$

Scattered light right after the scattering volume can be corrected as

$$I_{\text{solution,corr}} = I_{\text{solution}} \times 10^A \quad (11)$$

Therefore, the Rayleigh ratio (3) can be corrected as

$$R_{\theta} = \frac{10^{2A} I_{\text{solution}} / I_{0,\text{solution}} - I_{\text{solvent}} / I_{0,\text{solvent}}}{I_{\text{std}} / I_{0,\text{std}}} R_{\text{std}} \quad (12)$$

The Zimm plot of DPPDTT_1/CF after intensity correction is shown in Figure 2d (the Zimm plots of DPPDTT_2 & 3 are shown in Figure S3). One sees that the order of the curves as a function of concentration is now inverted to Figure 2c.

The calculated M_w and R_g are listed in Table 1 and a power-law relationship is observed between R_g and M_w (Figure 3)

$$R_g = k \times M_w^{0.98 \pm 0.05}$$

Table 1. GPC and SLS Results of DPPDTT in CF at 25 °C

| sample | DPPDTT_1 | DPPDTT_2 | DPPDTT_3 |
|---|----------|----------|----------|
| M_w^a (10^3 g/mol) | 30 | 100 | 150 |
| PDI ^a | 2.2 | 3.0 | 2.5 |
| M_w (10^3 g/mol) | 105 | 114 | 166 |
| R_g (nm) | 17.2 | 18.2 | 26.7 |
| A_2 (10^{-6} mL·mol/g ²) | −4.4 | −3.5 | −0.50 |

^aMeasured by GPC using 1,2,4-trichlorobenzene as the solvent and PS as the calibration standard at 150 °C.

The power exponent of 0.98, close to 1, agrees well with a rod-like object, which is consistent with and complements the results of SANS. The second virial coefficient A_2 is negative for all samples. Generally, if A_2 is negative, then it means that there is a stronger attraction between the chains compared with that between the chain and solvent. Meanwhile, it indicates that the chains have the tendency of forming aggregation in the solution. Therefore, most frequently, good solvents are

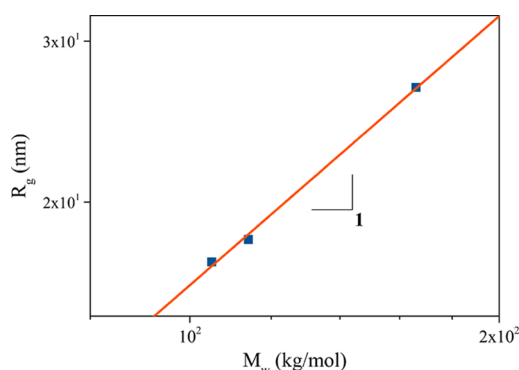


Figure 3. Relationship of R_h and M_w as measured by SLS.

preferred for SLS measurement ($A_2 > 0$). For our sample DPPDPTT in CF, the A_2 of the solution is negative but with a small magnitude of 10^{-6} mL·mol/g². The solution is relatively stable for a long time; therefore, the single-chain conformation is observed. Combining the above results, we deduce that DPPDPTT exists as isolated rod-like molecules in CF, no aggregate population being detected here by SLS.

Such a negative value of A_2 is at variance with positive values of A_2 reported so far for other conjugated polymers as listed in Table 2. As far as we know, DPPDPTT in CF is the first reported case of negative A_2 for conjugated polymers.

Table 2. The A_2 Values of Conjugated Polymers

| polymer | solvent | temperature | A_2 (mL·mol/g ²) | ref. |
|-----------------|------------------|-------------|--|-----------|
| P3HT | THF | 25 °C | 1.04×10^{-3} | 23 |
| | CF | 25 °C | 1.38×10^{-3} | |
| P3OT | CF | 25 °C | $(6.0\text{--}10.7) \times 10^{-4}$ | 24 |
| PPV derivatives | <i>p</i> -xylene | 50 °C | $(1.1\text{--}3.1) \times 10^{-4}$ | 16 |
| | toluene/nonane | | $(1.11\text{--}1.78) \times 10^{-5}$ | 52 |
| <i>cis</i> -PBO | MSA | 25 °C | $(3\text{--}6) \times 10^{-2}$ | 25 |
| PPE derivatives | THF | | positive | 26 |
| DP10-PPV | toluene | 25 °C | 3.7×10^{-6} | 32 |
| | CF | 25 °C | 6.7×10^{-6} | |
| DPPDPTT | CF | 25 °C | $(-0.5 \text{ to } -4.4) \times 10^{-6}$ | this work |

3.2. DLS of DPPDPTT in *o*-DCB. We now turn to the *o*-DCB solvent, in which, differently from CF, DPPDPTT can only dissolve at high temperatures (above 130 °C).^{11,46,53} Macroscopic aggregates are formed in the solution when stored at RT (~ 25 °C). In the Zimm plot of DPPDPTT₂/*o*-DCB solutions (1 h after being dissolved at 130 °C) at RT (Figure S4), an obvious upturn of the scattering intensity in low q values is observed; it further increases for increasing concentrations, which confirms the existence of aggregates. Meanwhile, for the same storage time, DLS still shows a single mode with a relaxation time around 5 ms (Figure 4a, 2 h). However, the relationship between Γ and q^2 of this fast mode, shown in Figure S5a, is only approximately linear, and the linear fit line does not pass through the origin. Let us have a closer look as a function of RT storage time, focusing on the changing trend of the hydrodynamic radius at a fixed small angle ($\theta = 20^\circ$).

As shown in Figure 4a, during storage, the plateau intensity increases gradually, and a slow relaxation mode appears after 40 h in DPPDPTT/*o*-DCB (0.15 g/L). The slow mode has a

relaxation time in the order of 1 s, which agrees with the appearance of large objects (aggregates). The corresponding hydrodynamic radius (R_h , assuming Einstein relation) of the solution during RT storage is shown in Figure 4b. The R_h of the fast mode increases gradually from ~ 25 to ~ 45 nm during the first 40 h. Then, another larger value of R_h appears: micrometer-sized aggregates are formed (a similar behavior for other concentrations is shown in Figure S6).

Figure 4c,d shows the effects of concentration. One fast relaxation mode (~ 5 ms) is observed for the samples with 0.05 and 0.10 g/L at a storage time of 53 h. Meanwhile, two relaxation modes are evident for the samples with higher concentrations (0.15 and 0.20 g/L). In line with common sense, the greater the concentration, the faster is the aggregation. The effective R_h of the solutions with different concentrations during RT storage is shown in Figure 5. The larger R_h with tens of micrometers appears in more concentrated solutions, while the smaller R_h keeps increasing toward ~ 50 nm.

To study the stability, structure, and intermolecular forces of such large-sized aggregates, we studied the heating process of the solution that has formed aggregates by storage at RT for 70 h. Figure 6a,b shows that in the slow heating process, two modes remain below 83 °C. When the temperature reaches 87 °C and is kept for 10 min, the slow mode gradually disappears. Bringing the solution back to RT, it takes over 20 h to get the micrometer-sized aggregates back, which are similar to the ones shown in Figure 4a.

Finally, we found it interesting to check the effect of a mechanical stimulus, by hand shaking a DPPDPTT/*o*-DCB solution with aggregates (at 0.15 g/L; a similar behavior for the other concentrations is shown in Figure S7). Indeed, attractive forces may not overpower the repulsive forces at low molecular distances enough to bring the species irreversibly at the lowest distances (“primary minimum”) but only in a so-called “secondary energy minimum”, where particles are loosely localized. The effect of shaking was studied in former works.³¹ As shown in Figure 6c (0 min), the slow mode disappeared immediately after shaking, and it reappeared after 20 min of storage, much quicker than that of the heated solution (30 h). As can be seen in Figure 6d, there is no significant change in R_h corresponding to the fast mode during storage.

3.3. UV–vis Spectra. To further study the changes in the intermolecular forces during the structural evolution, in situ UV–vis measurements were conducted on DPPDPTT/*o*-DCB solutions. In the heating process, UV–vis spectra exhibit a blueshift of the strongest peak from 830 to 815 nm (Figure 7a); meanwhile, the intensity of that peak gradually decreases. Although the origin of the dual band in the region of 700–850 nm remains controversial,⁵⁴ a redshift of the longer wavelength caused by intermolecular coupling is frequently observed in conjugated polymers.^{38,55} One can thus infer that on the reverse, the blueshift during heating agrees with the decreased intermolecular coupling resulted from the dissolution of aggregates.^{38,56} Different from their temperature dependence, no dependence of UV–vis spectra upon shaking is shown in Figure 7b, indicating that the intermolecular π – π stacking remains unchanged.

3.4. SANS of DPPDPTT in *o*-DCB. SANS measurements are also performed on DPPDPTT/*o*-DCB-d⁴ to characterize the change in the characteristic size (Figure 8). Considering the scattering intensity, the concentration of the solution is selected as 10 g/L, which is closer to the concentration used

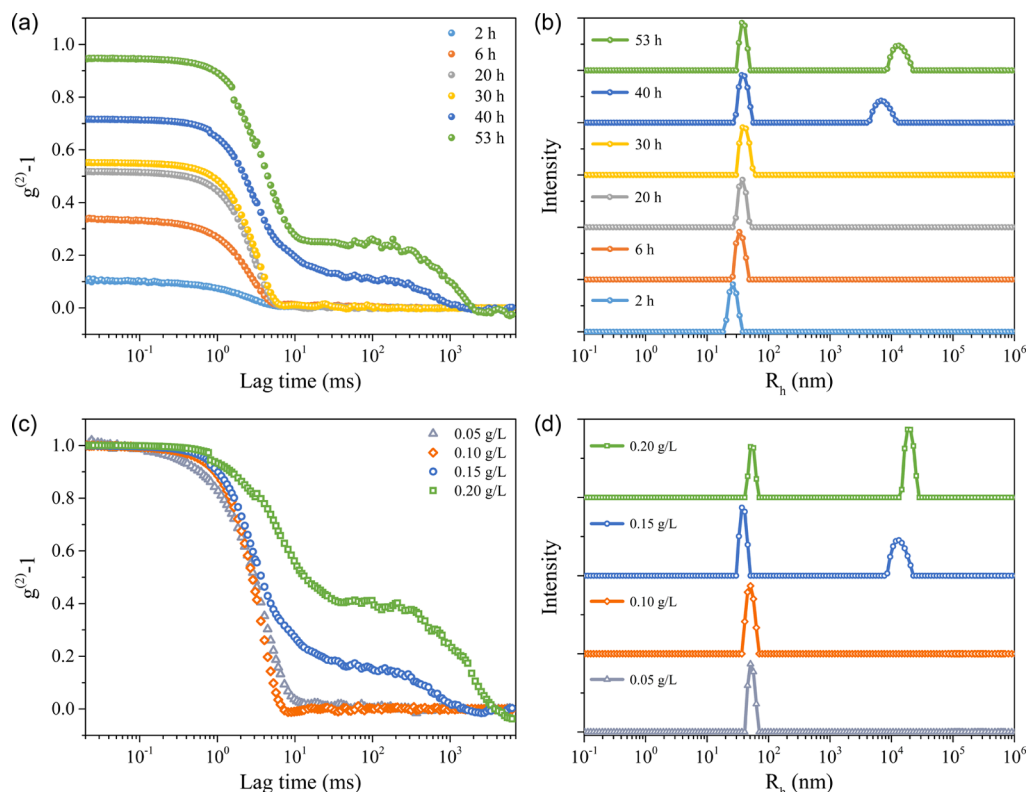


Figure 4. (a) Time-resolved autocorrelation function of DPPDTT_2 in *o*-DCB (0.15 g/L) stored at RT after dissolution at 130 °C and (b) corresponding distribution of R_h , (c) Normalized autocorrelation function of DPPDTT_2/*o*-DCB of four concentration solutions after storage at RT for 53 h and (d) corresponding distribution of R_h .

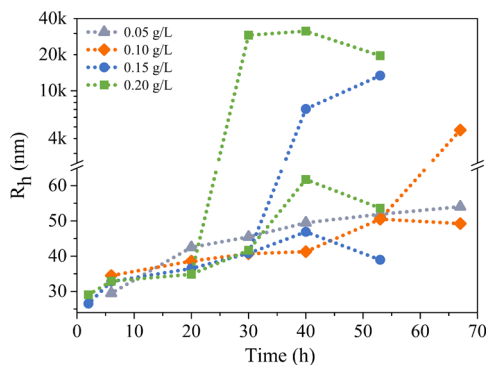


Figure 5. Hydrodynamic radius of solutions as a function of time during aging at RT (measured at $\theta = 20^\circ$).

for device processing. The “initial sample” is a nonflowing gel after cooling the solution, which was made at 130 °C down to RT and letting it stay overnight as shown in the photograph of Figure S2c. The heating and cooling processes of the solution were monitored by SANS. During heating, the scattering intensity decreases gradually at low q . Meanwhile, it remains almost unchanged at larger q . At 130 °C, the scattering intensity reaches the lowest value, but the shape of the curve is different from that of DPPDTT/CF-d. Instead of the constant slope at low q , seen in Figure 1b, the curve is flat, possibly corresponding to a Guinier region of the length of the cylinder. Indeed, the SANS curve measured at 130 °C can be fitted nicely with a cylinder form factor with a finite length. A comparison of the plots for CF (RT) and *o*-DCB (130 °C) can be found in Figure S8. A possible reason for the observed shorter length of the cylinder is the degradation of the polymer

during sample preparation as it has been staying at 130 °C for ~ 20 h because the cross-sectional radius is the same (~ 15 Å) both in chloroform (RT) and *o*-DCB (130 °C). In the cooling process, as long as the temperature stays above 80 °C, the scattering intensity at low q only increases slightly. A dramatic increase is seen when reaching 55 °C. Finally, at 29 °C, the scattering profile of the sample is very similar to that of the initial sample. In these cases, the SANS curves of the samples make visible two length scales, the diameter of chains corresponding to the fast drop at $q \approx 0.1$ Å $^{-1}$, and a length scale at lower q (~ 0.01 Å $^{-1}$). The reincrease of the local slope does not correspond to the attenuation due to the Guinier regime radius of gyration of the rod but better to some aggregated objects in the solution.

Hence, we fitted the data by a combination of two contributions, one visible mostly at high q , a cylinder form factor⁴⁷ (P_{cyl}) corresponding to the conformation of rod-like molecules, and one visible at low q , a parallelepiped form factor⁴⁸ (P_{para}) corresponding to the orderly π - π stacked backbones (ribbon-like). The details of these form factors are given in the Supporting Information. The parallelepiped form factor has been used in a previous study on the formation of aggregates of DPPDTT by introducing nonsolvents into the solution.⁵⁷ The fitting curves are displayed in Figure 8, and the parameters used are listed in Table 3. The radius of the rod remains unchanged during temperature variation. The length of the ribbon is too large to be estimated with the available q range. The shorter sides of the ribbon are ~ 80 and ~ 360 Å, respectively, which roughly agrees with the typical size of the nanoribbons of conjugated polymers reported in the literature and also with the AFM results shown below. During heating, k_1

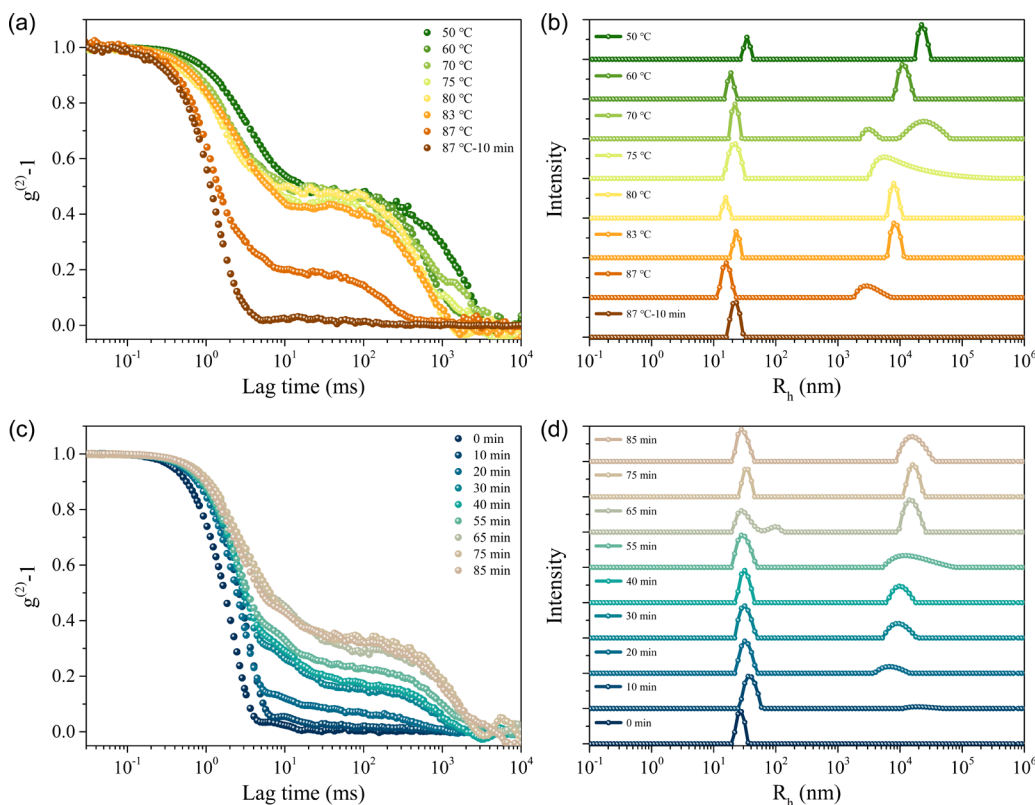


Figure 6. (a) Temperature dependence of the normalized autocorrelation function of DPPDTT_2/*o*-DCB (0.15 g/L, after storage at RT for 70 h, with aggregates) and (b) corresponding distribution of R_h . (c) Time-resolved normalized autocorrelation function of DPPDTT_2 in *o*-DCB (after shaking the initial aggregated solution in Figure 6a) and (d) corresponding distribution of R_h .

increases and k_2 decreases gradually, indicating the dissolution of aggregates into individual chains. The aggregation and dissolution processes are not fully reversible in kinetics: the aggregates disappear at 130 °C upon heating but reform at a much lower temperature (55 °C).

3.5. Schematic Diagram of Aggregation. The above light scattering and SANS results indicate that the assembly of conjugated polymers in solution is a process dependent on concentration, temperature, and time. Combining all information, it is possible to picture the formation of hierarchical structures of the DPPDTT/*o*-DCB system (Figure 9b). At the high temperature/low concentration limit, for example, 0.15 g/L above 87 °C or 10 g/L at 130 °C, the DPPDTT in *o*-DCB form “real” solutions with chains dispersed as isolated “rods” with a diameter of ~ 15 Å. During cooling, the chains are attached to each other due to the strong interchain interaction, resulting in “ribbon-like” aggregates (aggregation stage 1). Then, the ribbon-like aggregates tend to connect, forming micrometer-sized networks (aggregation stage 2). For more concentrated solutions (10 g/L), the whole system becomes a nonflowing defected gel containing ribbon-like assemblies with lateral characteristic lengths of 80 Å \times 400 Å.

Finally, a relation with the above-proposed picture can be found in morphology measurements. This has been done by AFM, yielding height images of the spin-coated sample (Figure 9a). They are the solid-state morphologies of spin-coated films from DPPDTT/*o*-DCB solutions with different aging times at RT (2, 30, and 53 h). The left AFM image was taken from spin-coated films of a solution with no aggregates, showing uniform nanoribbons with a width of ~ 50 nm. For a solution aged at RT for 30 h, loosely connected ribbons (~ 100 nm) are

observed. After aging for 53 h, micrometer-sized individual aggregates appear. Let us note that with respect to SANS, the AFM results shown here do not correspond to the same concentration.

The scales explored by AFM are closer to the ones of the above DLS results, but one must be cautious since a drying stage is involved. However, they confirm the picture of the progressive aggregation that we proposed. Finally, to end this multiscale investigation, let us point out that at an even larger scale, micrometer aggregates can be seen with the naked eye (Figure S2b).

Knowing the structure in solutions is important because it has a great influence on the microstructure of thin films. For example, the formation of an aggregated structure in DPPDTT when adding poor solvents can lead to an enhancement of hole mobilities in their OFET devices.⁵⁷ The strategy of “preaggregation” has been shown effective for controlling the microstructure of thin films to improve mobilities.^{43,58–60} While the charge transport within aggregates is effective, the interconnection between the aggregates is also crucial for long-distance charge transport.^{56,61} It remains challenging to identify and to tailor the best morphologies for performance. Therefore, the specific structure evolution of conjugated polymers at the different scales in solution must be considered during device processing.

The knowledge on the solution properties and manipulation of aggregation structures are not only critical for a controllable solution processing technology targeting industrial production of electronic devices but also important for understanding the origin of physical properties.⁶² Let us recall what has been observed, e.g., for P3ATs: chains assemble in solution into

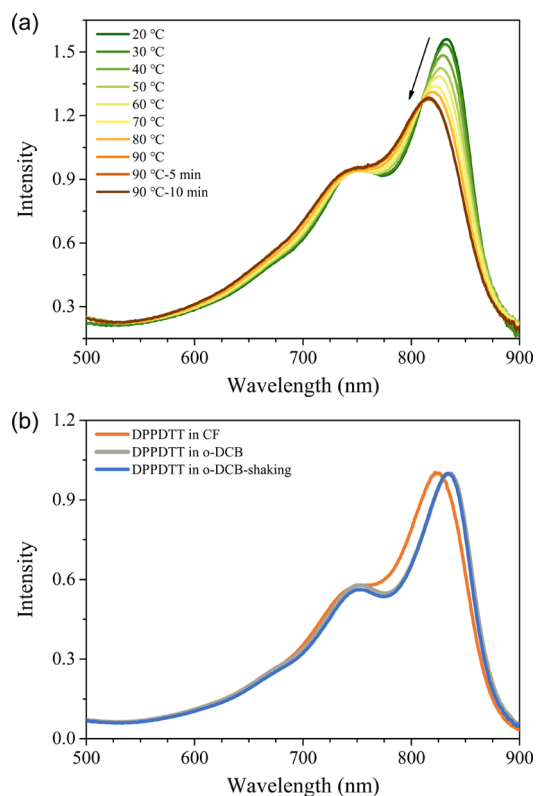


Figure 7. UV-vis spectra of DPPDTT/*o*-DCB (after storage at RT for 70 h, with aggregates) (a) at several temperatures in the heating process and (b) before/after shaking compared with DPPDTT/CF at RT.

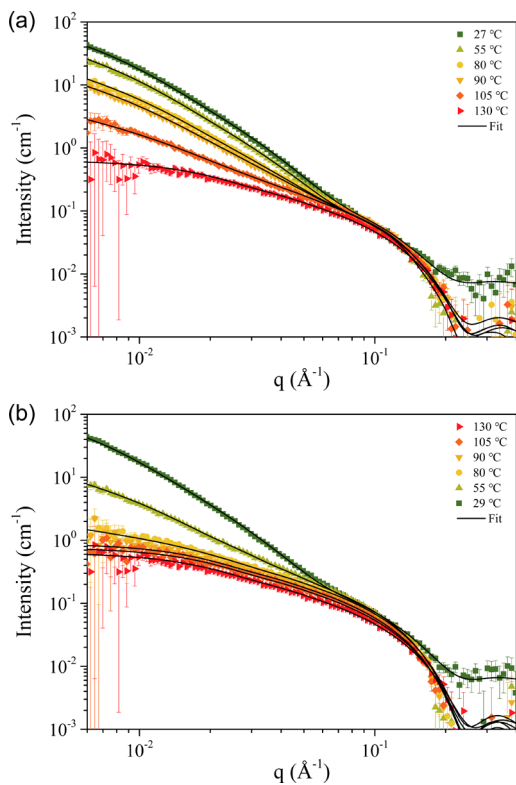


Figure 8. SANS curves of DPPDTT₃ in *o*-DCB-d⁴ (10 g/L) in (a) heating process and (b) cooling process.

Table 3. Fitting Parameters of the SANS Curves in Figure 8

| <i>T</i> (°C) | Heating | | | | Cooling | | | | | |
|---|------------|-------------|-------------|------------|-----------|-----------|-----------|-------------|-------------|-------------|
| | 27 | 55 | 80 | 90 | 105 | 130 | 90 | 80 | 55 | 29 |
| <i>k</i> ₁ × 10 ³ | 2.8 ± 0.1 | 2.9 ± 0.1 | 3.2 ± 0.1 | 3.2 ± 0.1 | 3.1 ± 0.1 | 2.7 ± 0.1 | 3.3 ± 0.1 | 3.8 ± 0.1 | 4.0 ± 0.1 | 3.5 ± 0.1 |
| <i>R</i> (Å) | 16 ± 1 | 16 ± 1 | 15 ± 1 | 15 ± 1 | 15 ± 1 | 14.5 ± 1 | 15.2 ± 1 | 15.2 ± 1 | 15.5 ± 1 | 15.0 ± 1 |
| <i>L</i> (Å) | 250 (fix) | 250 (fix) | 250 (fix) | 250 (fix) | 250 ± 50 | 250 ± 50 | 260 ± 50 | 250 ± 50 | 250 (fix) | 250 (fix) |
| <i>k</i> ₂ × 10 ³ | 2.3 ± 0.05 | 1.35 ± 0.05 | 0.67 ± 0.05 | 0.5 ± 0.05 | 0 | 0 | 0 | 0.03 ± 0.05 | 0.35 ± 0.05 | 1.95 ± 0.05 |
| <i>A</i> (Å) | 70 ± 20 | 80 ± 20 | 80 ± 20 | 80 ± 20 | 80 ± 20 | 80 ± 20 | 80 ± 20 | 80 ± 20 | 80 ± 20 | 80 ± 20 |
| <i>B</i> (Å) | 370 ± 90 | 360 ± 90 | 330 ± 80 | 330 ± 80 | 330 ± 80 | 330 ± 80 | 360 ± 90 | 360 ± 90 | 360 ± 90 | 420 ± 100 |
| <i>C</i> (Å) | ∞ | ∞ | ∞ | ∞ | ∞ | ∞ | ∞ | ∞ | ∞ | ∞ |

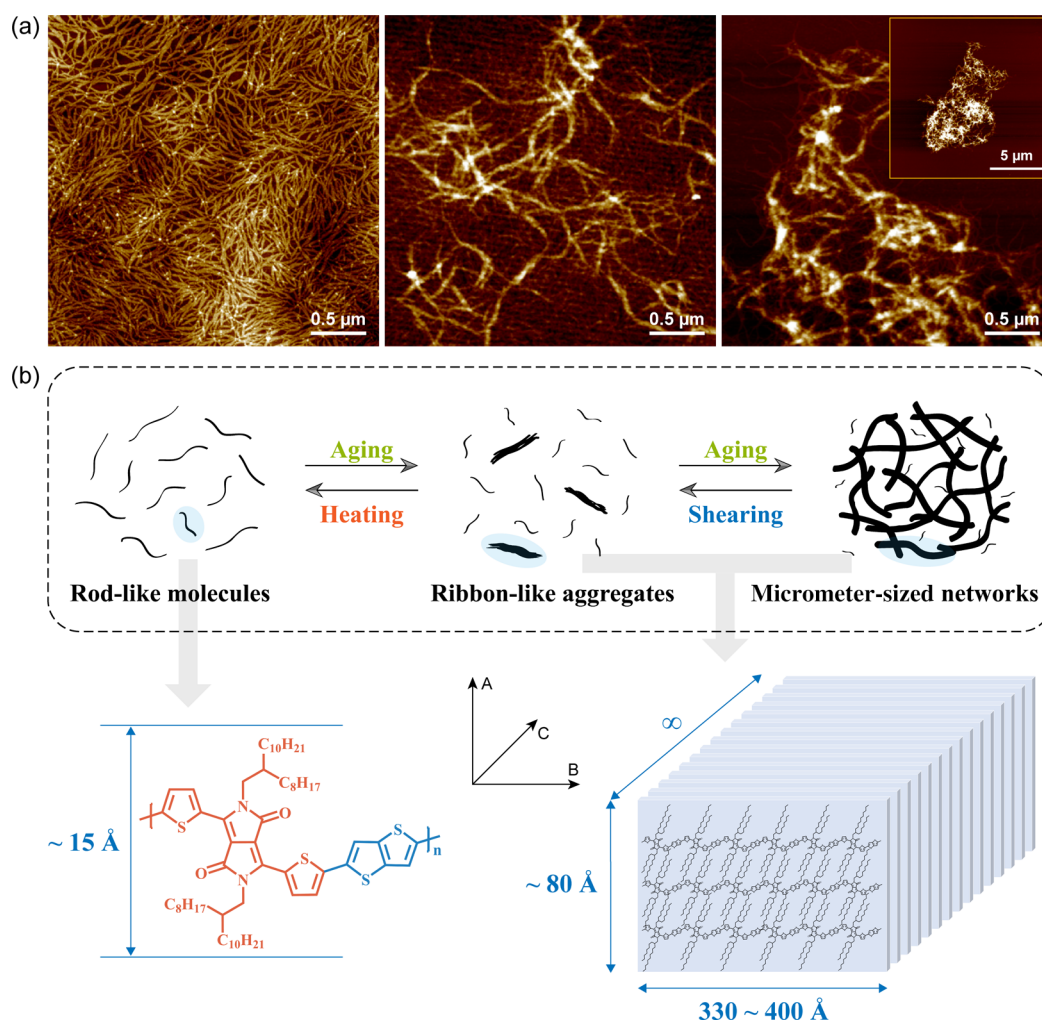


Figure 9. (a) AFM height images of solid-state films by spin-coating the DPPDTT_2/*o*-DCB solution (0.05 g/L) after storage at RT for 2, 30, and 53 h. The inset shows an image with lower magnification. (b) Schematic illustration representing the assembled structures (stacking) in the corresponding states of DPPDTT_2 in *o*-DCB.

nanofibers,^{63,64} nanowhiskers and nanoribbons,⁶⁵ and, ultimately, single crystals.^{66–69} Those assemblies exhibit higher crystalline order and closer π – π stacking, to which are attributed higher conductivity and mobility.^{63,65,70} Despite the technical difficulty, devices based on single crystals have been fabricated and characterized,^{63,66} showing exciting potentials of ultrahigh performance. While the global and local conformation of chains would be largely retained in the solid films for amorphous or poorly crystalline polymers, the local conformation may have remarkable changes after crystallization for highly crystalline polymers. A previous study already indicated hints about the equilibration of conformation during solvent vapor annealing.⁷¹

4. CONCLUSIONS

In summary, we have studied DPPDTT solution structures: (i) in CF at RT or in *o*-DCB at 130 °C, the chain exhibits rod-like conformation without aggregation, though negative A_2 in the order of $\sim 10^{-6}$ mL·mol/g² in CF indicates a net moderate attractive interaction between chains; (ii) in bad solvent *o*-DCB at RT, DPPDTT forms interesting aggregated structures in a two-stage process. A network is formed first out of ribbon-like heterogeneities with lateral characteristic lengths 80 Å × 400 Å. This first stage causes a gradual growth of R_h . Those

primary aggregates stick progressively to each other and form loosely packed objects, up to a micrometer scale, for which they become sensitive to a mechanical stimulus. We believe that the above results provide a general physical picture of how the chains of conjugated polymers behave in solution. The multiscale kinetic exploration is a powerful tool to understand how the final structure can be tuned.

■ ASSOCIATED CONTENT

Supporting Information

The Supporting Information is available free of charge at <https://pubs.acs.org/doi/10.1021/acs.macromol.0c01646>.

Details of sample preparation, formula of form factors for SANS fitting, and supporting data of the studied system (PDF)

■ AUTHOR INFORMATION

Corresponding Authors

Guoming Liu – CAS Key Laboratory of Engineering Plastics, CAS Research/Education Center for Excellence in Molecular Sciences, Institute of Chemistry, Chinese Academy of Sciences, Beijing 100190, China; University of Chinese Academy of

Sciences, Beijing 100049, China; orcid.org/0000-0003-2808-2661; Email: gmliu@iccas.ac.cn

François Boué – Laboratoire Léon Brillouin, 91191 Gif-sur-Yvette, France; Email: francois.boue@cea.fr

Authors

Chang Liu – CAS Key Laboratory of Engineering Plastics, CAS Research/Education Center for Excellence in Molecular Sciences, Institute of Chemistry, Chinese Academy of Sciences, Beijing 100190, China; University of Chinese Academy of Sciences, Beijing 100049, China

Wenxian Hu – CAS Key Laboratory of Engineering Plastics, CAS Research/Education Center for Excellence in Molecular Sciences, Institute of Chemistry, Chinese Academy of Sciences, Beijing 100190, China; University of Chinese Academy of Sciences, Beijing 100049, China

Hanqiu Jiang – Spallation Neutron Source Science Centre, Dongguan 523803, China

Charles C. Han – CAS Key Laboratory of Engineering Plastics, CAS Research/Education Center for Excellence in Molecular Sciences, Institute of Chemistry, Chinese Academy of Sciences, Beijing 100190, China

Henning Sirringhaus – Optoelectronics Group, Cavendish Laboratory, University of Cambridge, Cambridge CB3 0HE, United Kingdom; orcid.org/0000-0001-9827-6061

Dujin Wang – CAS Key Laboratory of Engineering Plastics, CAS Research/Education Center for Excellence in Molecular Sciences, Institute of Chemistry, Chinese Academy of Sciences, Beijing 100190, China; University of Chinese Academy of Sciences, Beijing 100049, China; orcid.org/0000-0002-2063-0873

Complete contact information is available at: <https://pubs.acs.org/10.1021/acs.macromol.0c01646>

Notes

The authors declare no competing financial interest.

ACKNOWLEDGMENTS

This work is supported by the National Natural Science Foundation of China (21922308). G.L. is grateful to the Royal Society (Newton Fellowship, NF151515) and the Youth Innovation Promotion Association of the Chinese Academy of Sciences (Y201908). F.B. thanks the support from the CAS President's International Fellowship Initiative (PIFI) (2018VMA0012). C.L. thanks Dr. Kuo Chen for the assistance in SLS/DLS experiments. SANS measurements were performed on the small-angle neutron scattering (SANS) instrument at the China Spallation Neutron Source (CSNS), Dongguan, China.

REFERENCES

(1) Burroughes, J. H.; Bradley, D. D. C.; Brown, A. R.; Marks, R. N.; Mackay, K.; Friend, R. H.; Burns, P. L.; Holmes, A. B. Light-emitting diodes based on conjugated polymers. *Nature* **1990**, *347*, 539–541.

(2) Yu, G.; Gao, J.; Hummelen, J. C.; Wudl, F.; Heeger, A. J. Polymer Photovoltaic Cells: Enhanced Efficiencies via a Network of Internal Donor-Acceptor Heterojunctions. *Science* **1995**, *270*, 1789.

(3) Sirringhaus, H.; Brown, P. J.; Friend, R. H.; Nielsen, M. M.; Bechgaard, K.; Langeveld-Voss, B. M. W.; Spiering, A. J. H.; Janssen, R. A. J.; Meijer, E. W.; Herwig, P.; de Leeuw, D. M. Two-dimensional charge transport in self-organized, high-mobility conjugated polymers. *Nature* **1999**, *401*, 685–688.

(4) Sirringhaus, H. 25th Anniversary Article: Organic Field-Effect Transistors: The Path Beyond Amorphous Silicon. *Adv. Mater.* **2014**, *26*, 1319–1335.

(5) Salleo, A.; Kline, R. J.; DeLongchamp, D. M.; Chabinyc, M. L. Microstructural Characterization and Charge Transport in Thin Films of Conjugated Polymers. *Adv. Mater.* **2010**, *22*, 3812–3838.

(6) Seki, S.; Tsukuda, S.; Tagawa, S.; Sugimoto, M. Correlation between Roughness of Nanowires and Polymer Backbone Conformation. *Macromolecules* **2006**, *39*, 7446–7450.

(7) Noriega, R.; Salleo, A.; Spakowitz, A. J. Chain conformations dictate multiscale charge transport phenomena in disordered semiconducting polymers. *Proc. Natl. Acad. Sci. U. S. A.* **2013**, *110*, 16315.

(8) Carbone, P.; Troisi, A. Charge Diffusion in Semiconducting Polymers: Analytical Relation between Polymer Rigidity and Time Scales for Intrachain and Interchain Hopping. *J. Phys. Chem. Lett.* **2014**, *5*, 2637–2641.

(9) Zhang, W.; Gomez, E. D.; Milner, S. T. Predicting Chain Dimensions of Semiflexible Polymers from Dihedral Potentials. *Macromolecules* **2014**, *47*, 6453–6461.

(10) Kuei, B.; Gomez, E. D. Chain conformations and phase behavior of conjugated polymers. *Soft Matter* **2017**, *13*, 49–67.

(11) Venkateshvaran, D.; Nikolka, M.; Sadhanala, A.; Lemaire, V.; Zelazny, M.; Kepa, M.; Hurhangee, M.; Kronemeijer, A. J.; Pecunia, V.; Nasrallah, I.; Romanov, I.; Broch, K.; McCulloch, I.; Emin, D.; Olivier, Y.; Cornil, J.; Beljonne, D.; Sirringhaus, H. Approaching disorder-free transport in high-mobility conjugated polymers. *Nature* **2014**, *515*, 384–388.

(12) Vezie, M. S.; Few, S.; Meager, I.; Pieridou, G.; Dörfling, B.; Ashraf, R. S.; Goñi, A. R.; Bronstein, H.; McCulloch, I.; Hayes, S. C.; Campoy-Quiles, M.; Nelson, J. Exploring the origin of high optical absorption in conjugated polymers. *Nat. Mater.* **2016**, *15*, 746–753.

(13) Hestand, N. J.; Spano, F. C. The Effect of Chain Bending on the Photophysical Properties of Conjugated Polymers. *J. Phys. Chem. B* **2014**, *118*, 8352–8363.

(14) Jackson, N. E.; Kohlstedt, K. L.; Savoie, B. M.; de la Cruz, M. O.; Schatz, G. C.; Chen, L. X.; Ratner, M. A. Conformational Order in Aggregates of Conjugated Polymers. *J. Am. Chem. Soc.* **2015**, *137*, 6254–6262.

(15) Lu, Y.; Yu, Z.-D.; Zhang, R.-Z.; Yao, Z.-F.; You, H.-Y.; Jiang, L.; Un, H.-I.; Dong, B.-W.; Xiong, M.; Wang, J.-Y.; Pei, J. Rigid Coplanar Polymers for Stable n-Type Polymer Thermoelectrics. *Angew. Chem., Int. Ed.* **2019**, *58*, 11390–11394.

(16) Gettinger, C. L.; Heeger, A. J.; Drake, J. M.; Pine, D. J. A photoluminescence study of poly(phenylene vinylene) derivatives: The effect of intrinsic persistence length. *J. Chem. Phys.* **1994**, *101*, 1673–1678.

(17) Aimé, J. P.; Bargain, F.; Schott, M.; Eckhardt, H.; Elsenbaumer, R. L.; Miller, G. G.; Mc Donnell, M. E.; Zero, K. Structural study of conducting polymers in solution. *Synth. Met.* **1989**, *28*, 407–417.

(18) Aime, J. P.; Bargain, F.; Schott, M.; Eckhardt, H.; Miller, G. G.; Elsenbaumer, R. L. Structural Study of Doped and Undoped Polythiophene in Solution by Small-Angle Neutron Scattering. *Phys. Rev. Lett.* **1989**, *62*, 55–58.

(19) Rawiso, M.; Aime, J.-P.; Fave, J. L.; Schott, M.; Müller, M. A.; Schmidt, M.; Baumgartl, H.; Wegner, G. Solutions of polydiacetylenes in good and poor solvents: a light and neutron scattering study. *J. Phys. France* **1988**, *49*, 861–880.

(20) Wignall, G. D.; Ballard, D. G. H.; Schelten, J. Measurements of persistence length and temperature dependence of the radius of gyration in bulk atactic polystyrene. *Eur. Polym. J.* **1974**, *10*, 861–865.

(21) Brûlet, A.; Boué, F.; Cotton, J. P. About the Experimental Determination of the Persistence Length of Wormlike Chains of Polystyrene. *J. Phys. II France* **1996**, *6*, 885–891.

(22) McCulloch, B.; Ho, V.; Hoarfrost, M.; Stanley, C.; Do, C.; Heller, W. T.; Segalman, R. A. Polymer Chain Shape of Poly(3-alkylthiophenes) in Solution Using Small-Angle Neutron Scattering. *Macromolecules* **2013**, *46*, 1899–1907.

- (23) Heffner, G. W.; Pearson, D. S. Molecular characterization of poly(3-hexylthiophene). *Macromolecules* **1991**, *24*, 6295–6299.
- (24) Heffner, G. W.; Pearson, D. S.; Gettinger, C. L. Characterization of poly(3-octylthiophene). I: Molecular characterization in dilute solution. *Polym. Eng. Sci.* **1995**, *35*, 860–867.
- (25) Roitman, D. B.; Wessling, R. A.; McAlister, J. Characterization of poly(p-phenylene-cis-benzobisoxazole) in methanesulfonic acid. *Macromolecules* **1993**, *26*, 5174–5184.
- (26) Cotts, P. M.; Swager, T. M.; Zhou, Q. Equilibrium Flexibility of a Rigid Linear Conjugated Polymer. *Macromolecules* **1996**, *29*, 7323–7328.
- (27) Farmer, B. L.; Chapman, B. R.; Dudis, D. S.; Adams, W. W. Molecular dynamics of rigid rod polymers. *Polymer* **1993**, *34*, 1588–1601.
- (28) Lukyanov, A.; Malafeev, A.; Ivanov, V.; Chen, H.-L.; Kremer, K.; Andrienko, D. Solvated poly-(phenylene vinylene) derivatives: conformational structure and aggregation behavior. *J. Mater. Chem.* **2010**, *20*, 10475–10485.
- (29) Li, Q.-y.; Lei, T.; Yao, Z.-f.; Wang, J.-y.; Pei, J. Multi-level Self-assembly of Conjugated Polymers. *Acta Polym. Sin.* **2019**, *50*, 1–12.
- (30) Hoeben, F. J. M.; Jonkheijm, P.; Meijer, E. W.; Schenning, A. P. H. J. About Supramolecular Assemblies of π -Conjugated Systems. *Chem. Rev.* **2005**, *105*, 1491–1546.
- (31) Perahia, D.; Traiphol, R.; Bunz, U. H. F. From single molecules to aggregates to gels in dilute solution: Self-organization of nanoscale rodlike molecules. *J. Chem. Phys.* **2002**, *117*, 1827–1832.
- (32) Li, Y.-C.; Chen, C.-Y.; Chang, Y.-X.; Chuang, P.-Y.; Chen, J.-H.; Chen, H.-L.; Hsu, C.-S.; Ivanov, V. A.; Khalatur, P. G.; Chen, S.-A. Scattering Study of the Conformational Structure and Aggregation Behavior of a Conjugated Polymer Solution. *Langmuir* **2009**, *25*, 4668–4677.
- (33) Li, Y.-C.; Chen, K.-B.; Chen, H.-L.; Hsu, C.-S.; Tsao, C.-S.; Chen, J.-H.; Chen, S.-A. Fractal Aggregates of Conjugated Polymer in Solution State. *Langmuir* **2006**, *22*, 11009–11015.
- (34) Huang, Y.; Cheng, H.; Han, C. C. Temperature Induced Structure Evolution of Regioregular Poly(3-hexylthiophene) in Dilute Solution and its Influence on Thin Film Morphology. *Macromolecules* **2010**, *43*, 10031–10037.
- (35) Huang, Y.; Cheng, H.; Han, C. C. Unimer–Aggregate Equilibrium to Large Scale Association of Regioregular Poly(3-hexylthiophene) in THF Solution. *Macromolecules* **2011**, *44*, 5020–5026.
- (36) Schmidt, K.; Tassone, C. J.; Niskala, J. R.; Yiu, A. T.; Lee, O. P.; Weiss, T. M.; Wang, C.; Fréchet, J. M. J.; Beaujuge, P. M.; Toney, M. F. A Mechanistic Understanding of Processing Additive-Induced Efficiency Enhancement in Bulk Heterojunction Organic Solar Cells. *Adv. Mater.* **2014**, *26*, 300–305.
- (37) Nguyen, T.-Q.; Doan, V.; Schwartz, B. J. Conjugated polymer aggregates in solution: Control of interchain interactions. *J. Chem. Phys.* **1999**, *110*, 4068–4078.
- (38) Qian, D.; Ye, L.; Zhang, M.; Liang, Y.; Li, L.; Huang, Y.; Guo, X.; Zhang, S.; Tan, Z.-a.; Hou, J. Design, Application, and Morphology Study of a New Photovoltaic Polymer with Strong Aggregation in Solution State. *Macromolecules* **2012**, *45*, 9611–9617.
- (39) Li, M.; Bin, H.; Jiao, X.; Wienk, M. M.; Yan, H.; Janssen, R. A. J. Controlling the Microstructure of Conjugated Polymers in High-Mobility Monolayer Transistors via the Dissolution Temperature. *Angew. Chem., Int. Ed.* **2020**, *59*, 846–852.
- (40) Zhang, H.; Li, T.; Ma, T.; Liu, B.; Ren, J.; Lin, J.; Yu, M.; Xie, L.; Lu, D. Effect of Solvents on the Solution State and Film Condensed State Structures of a Polyfluorene Conjugated Polymer in the Dynamic Evolution Process from Solution to Film. *J. Phys. Chem. C* **2019**, *123*, 27317–27326.
- (41) Chen, M. S.; Lee, O. P.; Niskala, J. R.; Yiu, A. T.; Tassone, C. J.; Schmidt, K.; Beaujuge, P. M.; Onishi, S. S.; Toney, M. F.; Zettl, A.; Fréchet, J. M. J. Enhanced Solid-State Order and Field-Effect Hole Mobility through Control of Nanoscale Polymer Aggregation. *J. Am. Chem. Soc.* **2013**, *135*, 19229–19236.
- (42) Fazzi, D.; Caironi, M. Multi-length-scale relationships between the polymer molecular structure and charge transport: the case of poly-naphthalene diimide bithiophene. *Phys. Chem. Chem. Phys.* **2015**, *17*, 8573–8590.
- (43) Kim, N.-K.; Jang, S.-Y.; Pace, G.; Caironi, M.; Park, W.-T.; Khim, D.; Kim, J.; Kim, D.-Y.; Noh, Y.-Y. High-Performance Organic Field-Effect Transistors with Directionally Aligned Conjugated Polymer Film Deposited from Pre-Aggregated Solution. *Chem. Mater.* **2015**, *27*, 8345–8353.
- (44) Zhou, P.; Zhang, Z.-G.; Li, Y.; Chen, X.; Qin, J. Thiophene-Fused Benzothiadiazole: A Strong Electron-Acceptor Unit to Build D–A Copolymer for Highly Efficient Polymer Solar Cells. *Chem. Mater.* **2014**, *26*, 3495–3501.
- (45) Reid, D. R.; Jackson, N. E.; Bourque, A. J.; Snyder, C. R.; Jones, R. L.; de Pablo, J. J. Aggregation and Solubility of a Model Conjugated Donor–Acceptor Polymer. *J. Phys. Chem. Lett.* **2018**, *9*, 4802–4807.
- (46) Li, Y.; Singh, S. P.; Sonar, P. A High Mobility P-Type DPP-Thieno[3,2-b]thiophene Copolymer for Organic Thin-Film Transistors. *Adv. Mater.* **2010**, *22*, 4862–4866.
- (47) Pedersen, J. S. Analysis of small-angle scattering data from colloids and polymer solutions: modeling and least-squares fitting. *Adv. Colloid Interface Sci.* **1997**, *70*, 171–210.
- (48) Nayuk, R.; Huber, K. Formfactors of Hollow and Massive Rectangular Parallelepipeds at Variable Degree of Anisotropy. *Z. Phys. Chem.* **2012**, *226*, 837–854.
- (49) Huglin, M. B. *Light scattering from polymer solutions*; Academic Press Inc.: London, 1972.
- (50) Berne, B. J.; Pecora, R. *Dynamic Light Scattering*; John Wiley: New York, 1976.
- (51) Chu, B. *Laser light scattering : basic principles and practice*; 2nd ed. ed.; Academic press: Boston (Mass.), 1991.
- (52) Chen, J.-H.; Chiu, C.-W.; Chen, L.-C.; Lai, S.-Y.; Lee, C.-C. Conformational structure and aggregation behavior of poly[2-methoxy-5-(2-ethylhexyloxy)-1,4-phenylenevinylene] in toluene/nonane solutions. *Polymer* **2012**, *53*, 4843–4854.
- (53) Li, J.; Zhao, Y.; Tan, H. S.; Guo, Y.; Di, C.-A.; Yu, G.; Liu, Y.; Lin, M.; Lim, S. H.; Zhou, Y.; Su, H.; Ong, B. S. A stable solution-processed polymer semiconductor with record high-mobility for printed transistors. *Sci. Rep.* **2012**, *2*, 754.
- (54) Beaujuge, P. M.; Amb, C. M.; Reynolds, J. R. Spectral Engineering in π -Conjugated Polymers with Intramolecular Donor–Acceptor Interactions. *Acc. Chem. Res.* **2010**, *43*, 1396–1407.
- (55) Reichenberger, M.; Kroh, D.; Matrone, G. M. M.; Schötz, K.; Pröller, S.; Filonik, O.; Thordardottir, M. E.; Herzig, E. M.; Bässler, H.; Stingelin, N.; Köhler, A. Controlling aggregate formation in conjugated polymers by spin-coating below the critical temperature of the disorder–order transition. *J. Polym. Sci., Part B: Polym. Phys.* **2018**, *56*, 532–542.
- (56) Steyrlleuthner, R.; Schubert, M.; Howard, I.; Klaumünzer, B.; Schilling, K.; Chen, Z.; Saalfrank, P.; Laquai, F.; Facchetti, A.; Neher, D. Aggregation in a High-Mobility n-Type Low-Bandgap Copolymer with Implications on Semicrystalline Morphology. *J. Am. Chem. Soc.* **2012**, *134*, 18303–18317.
- (57) Xi, Y.; Wolf, C. M.; Pozzo, L. D. Self-assembly of donor–acceptor conjugated polymers induced by miscible ‘poor’ solvents. *Soft Matter* **2019**, *15*, 1799–1812.
- (58) Lee, W.-Y.; Giri, G.; Diao, Y.; Tassone, C. J.; Matthews, J. R.; Sorensen, M. L.; Mannsfeld, S. C. B.; Chen, W.-C.; Fong, H. H.; Tok, J. B. H.; Toney, M. F.; He, M.; Bao, Z. Effect of Non-Chlorinated Mixed Solvents on Charge Transport and Morphology of Solution-Processed Polymer Field-Effect Transistors. *Adv. Funct. Mater.* **2014**, *24*, 3524–3534.
- (59) Nahid, M. M.; Welford, A.; Gann, E.; Thomsen, L.; Sharma, K. P.; McNeill, C. R. Nature and Extent of Solution Aggregation Determines the Performance of P(NDI2OD-T2) Thin-Film Transistors. *Adv. Electron. Mater.* **2018**, *4*, 1700559.
- (60) Ouyang, G.; Wu, H.; Qiao, X.; Zhang, J.; Li, H. Modulating Surface Morphology and Thin-Film Transistor Performance of Bi-

thieno[3,4-c]pyrrole-4,6-dione-Based Polymer Semiconductor by Altering Preaggregation in Solution. *ACS Omega* **2018**, *3*, 9290–9295.

(61) Noriega, R.; Rivnay, J.; Vandewal, K.; Koch, F. P. V.; Stingelin, N.; Smith, P.; Toney, M. F.; Salleo, A. A general relationship between disorder, aggregation and charge transport in conjugated polymers. *Nat. Mater.* **2013**, *12*, 1038–1044.

(62) Lim, J. A.; Liu, F.; Ferdous, S.; Muthukumar, M.; Briseno, A. L. Polymer semiconductor crystals. *Mater. Today* **2010**, *13*, 14–24.

(63) Wang, S.; Kappl, M.; Liebewirth, I.; Müller, M.; Kirchhoff, K.; Pisula, W.; Müllen, K. Organic Field-Effect Transistors based on Highly Ordered Single Polymer Fibers. *Adv. Mater.* **2012**, *24*, 417–420.

(64) Oh, J. Y.; Shin, M.; Lee, T. I.; Jang, W. S.; Min, Y.; Myoung, J.-M.; Baik, H. K.; Jeong, U. Self-Seeded Growth of Poly(3-hexylthiophene) (P3HT) Nanofibrils by a Cycle of Cooling and Heating in Solutions. *Macromolecules* **2012**, *45*, 7504–7513.

(65) Liu, J.; Arif, M.; Zou, J.; Khondaker, S. I.; Zhai, L. Controlling Poly(3-hexylthiophene) Crystal Dimension: Nanowhiskers and Nanoribbons. *Macromolecules* **2009**, *42*, 9390–9393.

(66) Kim, D. H.; Han, J. T.; Park, Y. D.; Jang, Y.; Cho, J. H.; Hwang, M.; Cho, K. Single-Crystal Polythiophene Microwires Grown by Self-Assembly. *Adv. Mater.* **2006**, *18*, 719–723.

(67) Ma, Z.; Geng, Y.; Yan, D. Extended-chain lamellar packing of poly(3-butylthiophene) in single crystals. *Polymer* **2007**, *48*, 31–34.

(68) Xiao, X.; Hu, Z.; Wang, Z.; He, T. Study on the Single Crystals of Poly(3-octylthiophene) Induced by Solvent-Vapor Annealing. *J. Phys. Chem. B* **2009**, *113*, 14604–14610.

(69) Rahimi, K.; Botiz, I.; Stingelin, N.; Kayunkid, N.; Sommer, M.; Koch, F. P. V.; Nguyen, H.; Coulembier, O.; Dubois, P.; Brinkmann, M.; Reiter, G. Controllable Processes for Generating Large Single Crystals of Poly(3-hexylthiophene). *Angew. Chem., Int. Ed.* **2012**, *51*, 11131–11135.

(70) Han, W.; He, M.; Byun, M.; Li, B.; Lin, Z. Large-Scale Hierarchically Structured Conjugated Polymer Assemblies with Enhanced Electrical Conductivity. *Angew. Chem., Int. Ed.* **2013**, *52*, 2564–2568.

(71) Vogelsang, J.; Brazard, J.; Adachi, T.; Bolinger, J. C.; Barbara, P. F. Watching the Annealing Process One Polymer Chain at a Time. *Angew. Chem., Int. Ed.* **2011**, *50*, 2257–2261.